coatings

MDPI

Article

Corrosion Behavior of the Ti–6Al–4V Alloy in Sulfate-Reducing Bacteria Solution

Xingwei Zheng [1,2], Xin Zhuang [1], Yanhua Lei [3,*], Zhenhua Chu [1,*], Jingxiang Xu [1], Li Gao [1] and Xiaoming Sun [1]

1 College of Engineering Science and Technology, Shanghai Ocean University, Shanghai 201306, China; xwzheng@shou.edu.cn (X.Z.); m170650880@st.shou.edu.cn (X.Z.); jxxu@shou.edu.cn (J.X.); lgao@shou.edu.cn (L.G.); xmsun@shou.edu.cn (X.S.)

2 College of Science, Donghua University, Shanghai 201620, China

3 Institute of Marine Materials Science and Engineering, College of Ocean Science and Engineering, Shanghai Maritime University, Shanghai 201306, China

* Correspondence: yhlei@shmtu.edu.cn (Y.L.); zhchu@shou.edu.cn (Z.C.)

Received: 7 November 2019; Accepted: 17 December 2019; Published: 29 December 2019

Abstract: The corrosion behavior of the Ti–6Al–4V alloy was investigated in a sulfate-reducing bacteria (SRB) solution. The results showed that sulfate-reducing bacteria has good affinity with the surface of the Ti–6Al–4V alloy after 5 days. A potentiodynamic polarization test demonstrated that the corrosion resistance of the Ti–6Al–4V alloy was initially improved but deteriorated quickly in the subsequent period. The corrosion mechanism of the Ti–6Al–4V alloy was revealed by analyzing its microstructure with the aid of scanning electron microscopy, X-ray photoelectron spectroscopy and X-ray fluorescence. The pitting corrosion was deemed to be a typical cause of the corrosion behavior of the alloy in the SRB solution. The underlying mechanism of the pitting corrosion was proposed for the alloy.

Keywords: Ti–6Al–4V alloy; pitting corrosion; sulfate-reducing bacteria

1. Introduction

Corrosion is one of the primary causes that leads to the failure of components, negatively affecting human and machine systems [1]. Reportedly, every year, the financial loss directly due to corrosion occurring in the United States is about $276 billion in total. This amount is approximately 3.1% of the gross domestic product of the nation [2]. To date, the study of microbiologically influenced corrosion (MIC) has become an attractive topic because MIC is one of the main reasons attributed to the corrosive damage of metals [3–5]. Typically, sulfate-reducing bacteria (SRB) actively assume the role as corrosive bacteria that can erode most metallic materials (e.g., steel [6–8], aluminum alloy [6,7,9], and pure titanium [10]). Furthermore, external factors can also affect the corrosion rate of metals by SRB, such as stress [11] and Fe^{2+} in the SRB solution [12].

Characterized by high specific strength and excellent corrosion resistance, the Ti–6Al–4V alloy is the most often used titanium alloy serving in industries such as astronautic and aeronautic engineering, as well as biomedical engineering [13,14]. In recent decades, attention has been given to the applications of the Ti–6Al–4V alloy in marine engineering [15–17]. However, in the ocean setting, the alloy suffers damage caused by corrosion from seawater and MIC. To date, very few works have been reported about the corrosion of the Ti–6Al–4V alloy by SRB, although demonstrably titanium alloys are corrosion resistant in seawater [18]. In this paper, to develop the resistance to bacterial corrosion—and thus to promote the application of the Ti–6Al–4V alloy in marine engineering—the corrosion behavior of this alloy in SRB solution was investigated by means of surface analysis techniques and electrochemical methods.

2. Experimental Methods

2.1. Materials

The actual and nominal compositions of the Ti–6Al–4V alloy used in this work are listed in Table 1. Specimens (15 mm × 15 mm) used for the study were polished on silicon carbide papers with grit sizes up to 1000 before experiments.

Table 1. The compositions (wt.%) of titanium alloy.

Compositions	Al	V	Ti
Detail composition	5.61	3.72	Balance
Nominal composition	5.5%–6.75%	3.5%–4.5%	Balance

2.2. Corrosion Experiment with SRB

The strains of SRB used in the study were provided by the Guangdong Provincial Microbial Culture Collection Center (Guangdong, China). A modified Beer medium was used to cultivate SRB. The chemical composition of the medium is listed in Table 2.

Table 2. The chemical composition of the medium.

Composition	Mass (g)
$MgSO_4$	2
Sodium citrate	5
$CaSO_4{\cdot}2H_2O$	1
NH_4Cl	1
K_2HPO_4	0.5
Sodium lactate syrup	3.5
Yeast extract	1.0

The strains were inoculated into the medium with the suitable growth conditions for SRB to study its growth pattern. The growth curve of SRB was measured according to the McFarland standard proposed by German Bio Mérieux and Marcy L'Etoile [19].

A control set of Ti–6Al–4V alloy coupons exposed to sterilized SRB medium was also observed for a similar period of time.

2.3. Specimen Analysis

First, the specimens were soaked separately in SRB solution for 1, 3 and 5 days, and then they were examined by fluorescence microscopy (ECLIPSE Ti, Nikon, Japan) to observe the adsorption behavior of SRB on the surface of the Ti–6Al–4V alloy. The set of specimens was observed via scanning electron microscopy (S-4800, Hitachi, Tokyo, Japan) to record the presence of bacteria and morphological features of the corroded titanium alloy coupons. The variation of composition in the surface of titanium alloy coupons was detected by X-ray fluorescence (XRF, ZSX primus, Rigaku, Japan) after the immersion test. The specimens were also tested in artificial seawater by electrochemical workstation (CHI660E C17168, Chenhua, Shanghai, China) for an impedance spectrum and polarization curve. The final corrosion product was detected via X-ray photoelectron spectroscopy (XPS, EscaLab 250Xi, Thermo Fisher Scientific, Waltham, MA, USA).

3. Results and Discussion

3.1. The Adsorption Behavior of SRB

In order to maintain the activity of SRB during the experiment, it is necessary to investigate its growth behavior. Figure 1a shows the growth curve of SRB, revealing that the growth process of SRB

can be divided into three stages, i.e., slow growth phase, exponential growth phase, and stagnant growth phase. The study by Oguro concluded that the number of SRB reached the maximum after one day and began to decrease after three days [20]. Thus, the SRB in the test tubes was replaced with equal fresh SRB for every three days and the fresh SRB solution had been fostered for 1 day.

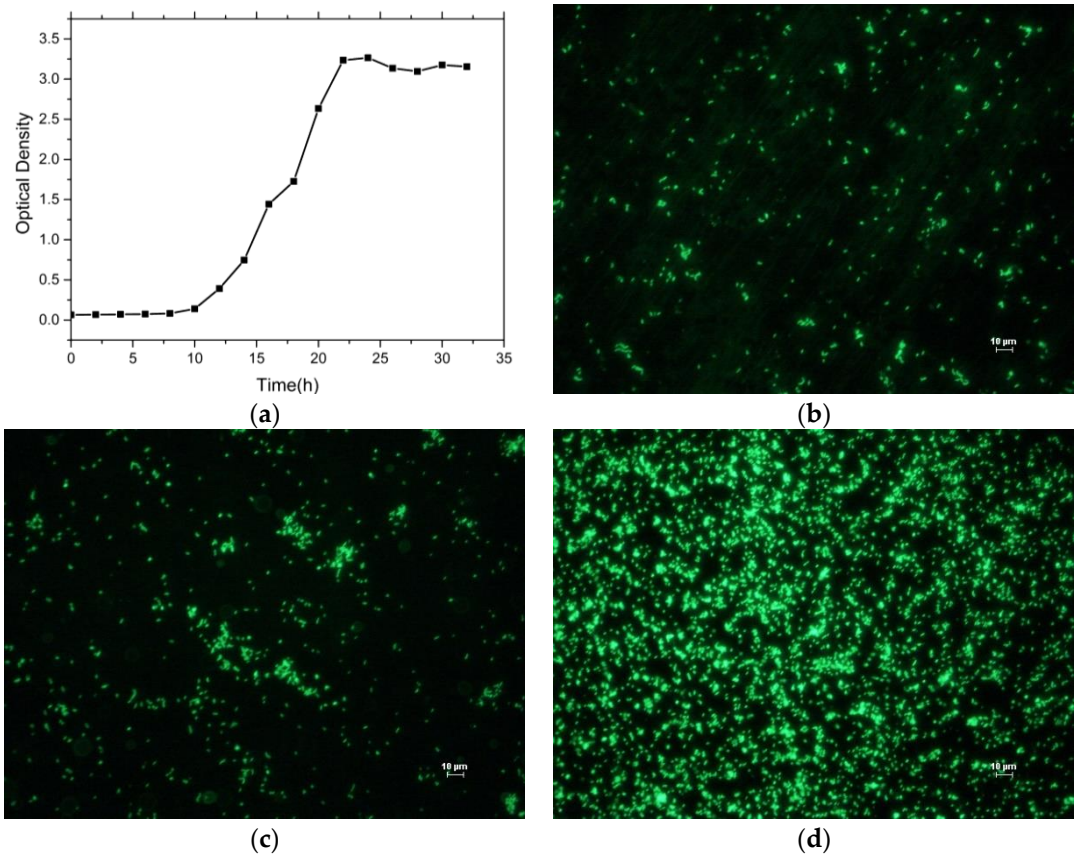

Figure 1. Sulfate-reducing bacteria (SRB) growth curve and its adsorption behavior. (**a**) Growth curve of the SRB, (**b**) the adsorption behavior of SRB for 1 day, (**c**) the adsorption behavior of SRB for 2 days, and (**d**) the adsorption behavior of SRB for 5 days.

The adsorption behavior of SRB on the surface of the Ti–6Al–4V alloy was observed by fluorescence microscope. Figure 1b shows a fluorescent microscopy picture revealing a little SRB on the titanium alloy surface for 1 day. Figure 1c shows more and more SRB on the titanium alloy surface; a few colonies had formed after 2 days. Figure 1d shows a large number of SRB on the titanium alloy surface and a number of colonies had formed during the five-day period. The results of fluorescence microscopy show that SRB are easily attached to titanium alloy surface.

3.2. Electrochemical Measurements

The electrochemical reactions of the titanium alloy in sulfate-reducing bacteria solution were investigated by potentiodynamic polarization and cyclic voltammetry measurements. Figure 2 shows the potentiodynamic polarization curves of the samples for different immersion time. The anodic current density levels off near −0.3 to ~0.4 V, demonstrating the passivation characteristics of the Ti–6Al–4V alloy in SRB solution. This passivation behavior was attributed to the formation of oxide films on the Ti–6Al–4V alloy surface. As the potential sweeps to more positive values, a substantial current becomes observable near 0.4 V, which is due to the oxygen evolution reactions [21]. Table 3 lists the values of the corrosion potential and the corrosion current density of the samples for different immersion times. The results reveal that the corrosion potential of the sample shifted positively first

and then negatively. The initial magnitude of the current density was at a magnitude of 10^{-7} A/cm^2, and then the current density maintained at a magnitude of 10^{-6} A/cm^2 finally rose to a magnitude of 10^{-5} A/cm^2, which indicates that the sample soaked in SRB for 31 days had been severely damaged. The value of current density is close to that of the Ti–6Al–4V alloy in NaCl solution [22]. On the other hand, it can be seen that the potential increased gradually, which demonstrates the corrosion resistance of the Ti–6Al–4V alloy in sulfate-reducing bacteria solution is enhanced at the initial stage. Then, the potential decreased rapidly, which demonstrates that the corrosion resistance of the Ti–6Al–4V alloy deteriorated greatly.

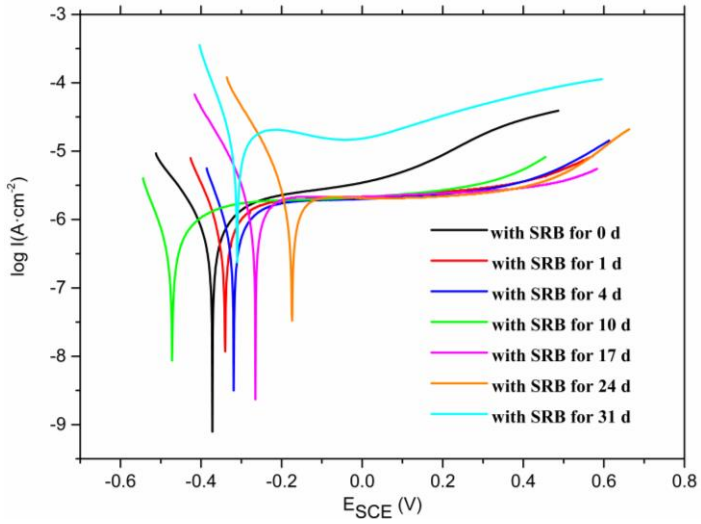

Figure 2. Potentiodynamic polarization curves of the samples for different immersion time.

Table 3. Polarization parameters of the samples for different immersion time.

The Samples for Different Immersion Time	Corrosion Potential (V)	Corrosion Current (A)
with SRB for 0 day	−0.374	3.715×10^{-7}
with SRB for 1 day	−0.356	7.161×10^{-7}
with SRB for 4 days	−0.331	5.741×10^{-7}
with SRB for 10 days	−0.481	3.564×10^{-7}
with SRB for 17 days	−0.253	1.023×10^{-6}
with SRB for 24 days	−0.162	1.288×10^{-6}
with SRB for 31 days	−0.321	1.188×10^{-5}

Figure 3a shows the Nyquist plots of impedance module for samples for different immersion times. Flat and incomplete capacitive arcs are shown in all Nyquist diagrams, which is consistent with the previous investigations [23–25]. The size of the arc increases as the soaking time increases and then decreases, which reveals the impedance amplitude also increased first (1–4 days) and then decreased. Figure 3c shows the log|Z|– log f (Z represents impedance and f represents frequency) diagram of Bode plots, revealing the impedance of the sample immersed in SRB for 31 days reduced significantly. Figure 3d shows the Ø – log f (Ø represents Phase) diagram of the Bode plots. It illustrates two time constants in the impedance spectrum for the last day: one in the low-frequency region and the other one in the middle frequency region. The time constant in the low frequency region indicates the charge transfer reaction occurring in the film electrolyte interface, and the time constant in the intermediate frequency region reflects the characteristics of the passivation layer.

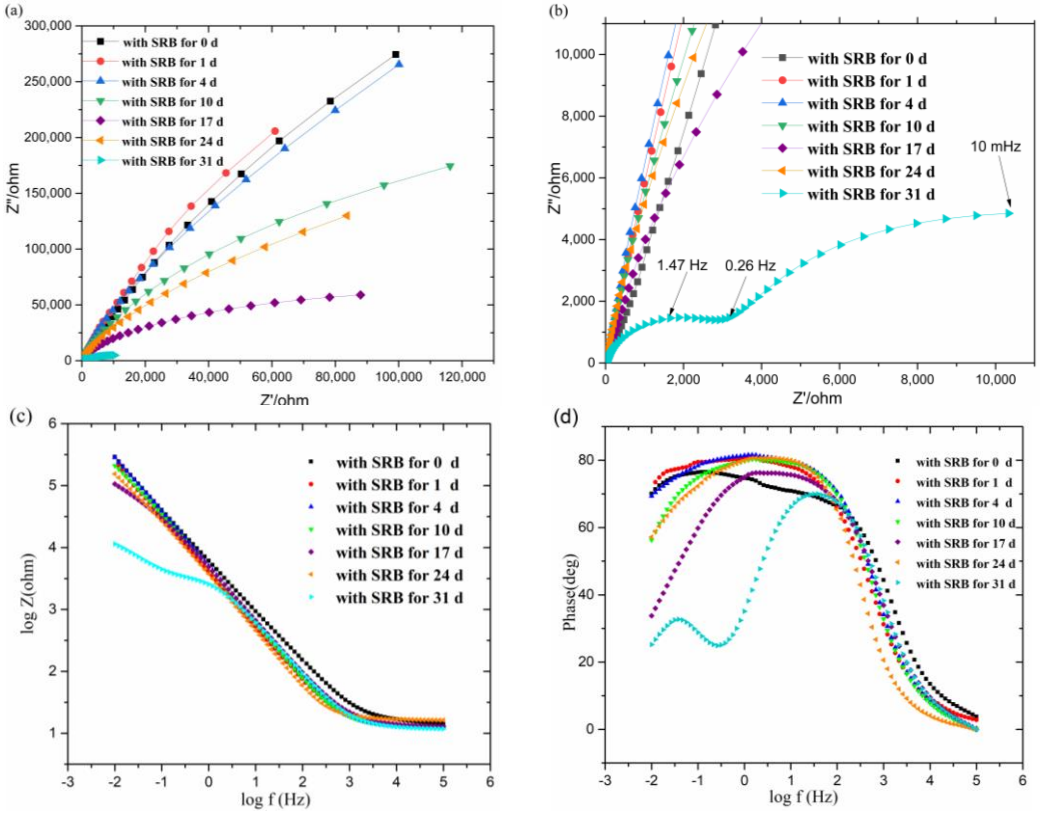

Figure 3. The electrochemical impedance spectroscopy (EIS) results for the titanium alloys in SRB solution (0–31 days). (**a**) Nyquist plots of impedance module for samples for different immersion time, (**b**) an enlarged view of the Nyquist diagram, (**c**) Bode plots (log|*Z*|– log *f*) of impedance module for samples for different immersion time, and (**d**) Bode plots (Ø – log *f*) of impedance module for samples for different immersion time.

According to the above results, the equivalent electronic circuits are shown in Figure 4, which are used to fit the EIS results. The fitting result is shown in Figure 5. It is likely that the fit of the capacitive reactance is fitted by the equivalent circuits and the original impedance spectrum is satisfactory, which explains that these equivalent circuits can represent the internal structures and reaction processes of the original electrochemical devices. R_s represents the electrolyte resistance, R_f and Q_f represent the resistance and capacitance of the titanium alloy matrix, and Q_{dl} represents the constant phase angle element of the outer layer of the oxide film. The simulation analysis of the capacitive elements involved in the time is replaced by constant phase elements (the symbol is Q). The specific expression of the constant phase elements is the following Expression (1) [26,27]. In this expression, Y_0 represents the admittance constant, ω represents angular frequency, j represents imaginary part, n represents the exponential term of the constant phase element, $0 < n < 1$, if $n = 1$, Q represents a pure capacitance, if $n = 0$, and Q represents a pure resistance.

$$Z_Q = \frac{1}{Y_0}(j\omega)^{-n} \quad (1)$$

The resistance data variation for the circuit elements is shown in Figure 6. The difference between the maximum and minimum values of R_f is 1.11×10^6 Ω·cm^2, but the difference between the maximum and minimum values of R_s is only about 6 Ω·cm^2. Therefore, the variation of R_s, compared with R_f, can be approximately assumed to remain unchanged. Subsequently, the variation of R_s has little effect on the experimental results. The value of the electrolyte resistance remained at a normal level, which is similar to previous research [18]. The titanium alloy matrix resistance R_f reduced slightly after soaking in SRB for 1 day, which indicates that the Ti–6Al–4V alloy had suffered slight damage. R_f dramatically

increased from 5.17×10^5 to the highest 1.11×10^6 and finally drastically decreased to 3.18×10^3, which depicts that passivation film was formed on the surface of the Ti–6Al–4V alloy at the beginning of immersion. Meanwhile, as the soaking time increases, the resistance will worsen.

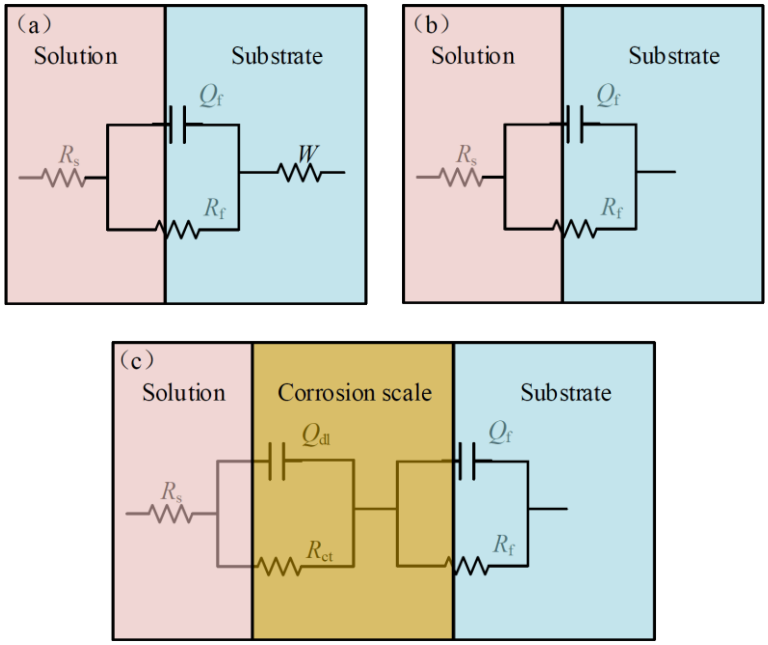

Figure 4. Equivalent circuits. (**a**) The equivalent circuit for 0, 1 and 4 days, (**b**) the equivalent circuit for 10, 17 and 24 days, and (**c**) the equivalent circuit for 31 days. (*W* represents Warburg impedance, R_{ct} represents polarization resistance, R_s represents the electrolyte resistance, R_f and Q_f represent the resistance and capacitance of the titanium alloy matrix, and Q_{dl} represents the constant phase angle element of the outer layer of the oxide film).

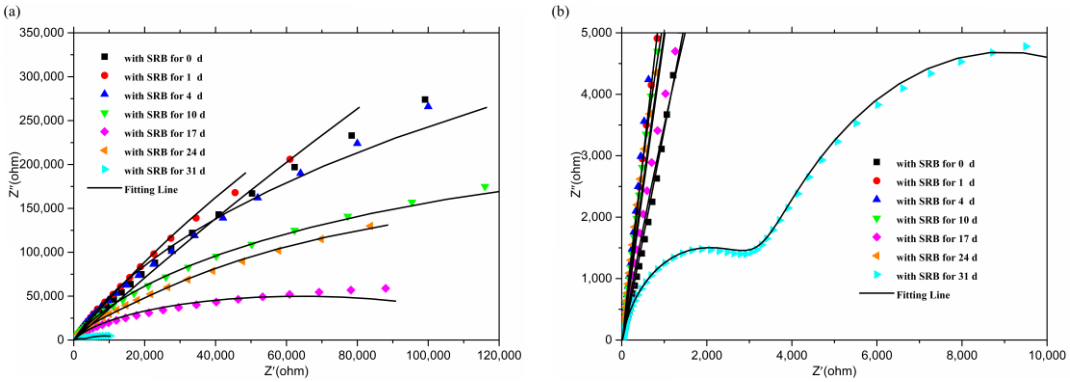

Figure 5. (**a**) The fitting result of each equivalent circuit and (**b**) the enlarged view of the fitting result of each equivalent circuit.

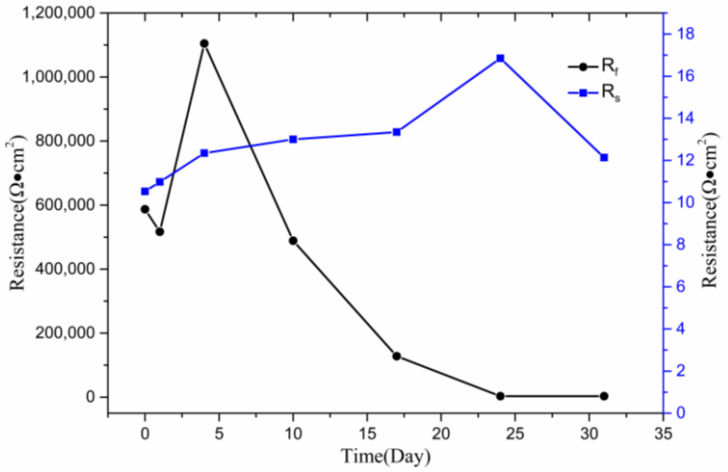

Figure 6. Parameters (resistance) change of equivalent circuits obtained by fitting the experimental results of EIS.

3.3. Surface Analysis

In order to investigate the effect of SRB on the corrosion of the Ti–6Al–4V alloy, the morphologies of the surfaces of the Ti–6Al–4V alloy exposed to SRB and artificial seawater without SRB were observed separately via a scanning electron microscope. Figure 7a shows the morphology of the Ti–6Al–4V alloy surface, which was soaked in SRB solution for 31 days. A number of rod-shaped SRB cells can be seen adsorbing on the surface of the Ti–6Al–4V alloy. Figure 7b shows the SEM picture of the morphology of the Ti–6Al–4V alloy surface after removing corrosion products, which reveals many micropits. The diameter is approximately 2 μm, which is similar to the corrosion pit of pure titanium in SRB [10]. Figure 7c shows the untreated Ti–6Al–4V alloy with a smooth surface. Figure 7d shows the surface of the Ti–6Al–4V alloy control coupon exposed to sterilized SRB medium for 31 days. There is almost no variation between the samples before and after immersion in the sterilized SRB medium for 31 days, while many micropits are observed on the surface after immersion in SRB solution. The above results show that the Ti–6Al–4V alloy exhibits excellent corrosion resistance in seawater, while the SRB can obviously accelerate the corrosion rate of the Ti–6Al–4V alloy.

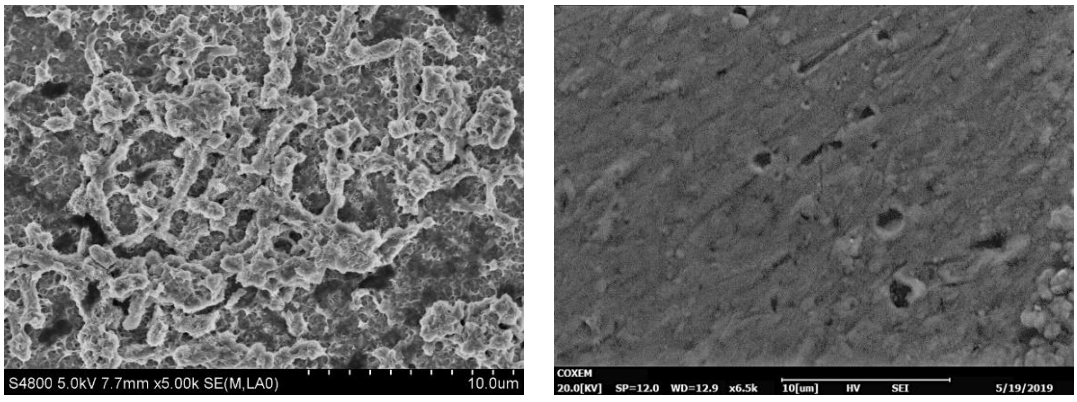

(**a**) (**b**)

Figure 7. *Cont.*

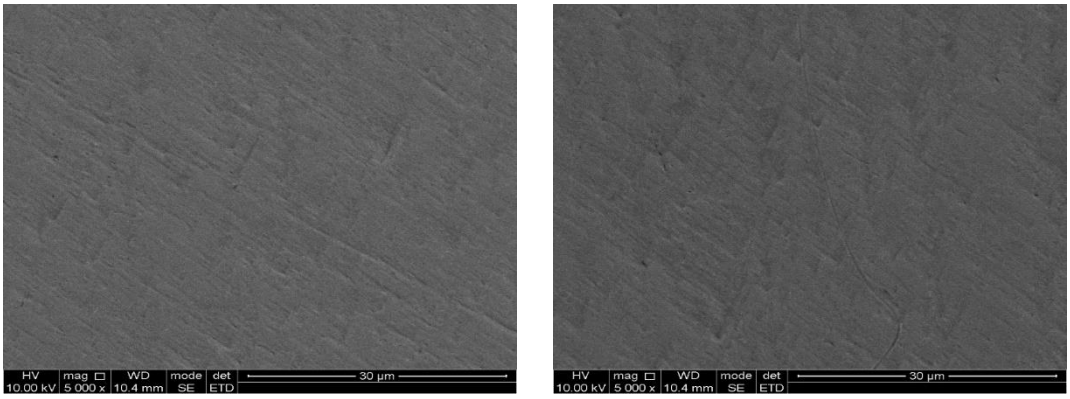

(**c**) (**d**)

Figure 7. Scanning electron microphotograph results. (**a**) Surface morphology of the Ti–6Al–4V alloy immersed in SRB solution for 31 days, (**b**) surface morphology of the Ti–6Al–4V alloy immersed in SRB solution for 31 days without corrosion products, (**c**) untreated sample, and (**d**) surface of the Ti–6Al–4V alloy coupon exposed to sterile water for 31 days.

In order to analyze the corrosion product of the Ti–6Al–4V alloy in SRB solution, the contents of various elements in each stage were measured by XRF. Table 4 provides the results of XRF, revealing sulfide with increasing mass fraction. The effects of sulfide on the passivation behavior of the Ti–6Al–4V alloy can be identified from the anodic branch of the potentiodynamic tests. It can be observed in the secondary passive region that the concentration of sulfide increases and the passive current densities shift positively as the immersion time increases. It is worthwhile to point out that the passive current densities for 4 and 10 days were smaller than that for 1 day, which means the sulfide cannot dissolve but rather stabilize the passivation film when a small amount of sulfide concentration is sufficiently high. This dual role of sulfides can be attributed to the dissolution processes caused by additional protons, and the dynamic competition of sulfur ions involved in the film formation, which is consistent with previous reports [18,28]. When the Ti–6Al–4V alloy was immersed in SRB solution, the TiO_2 protective film gradually formed on the surface of the matrix early [18]. Pourbaix [29] and Cocke [30] inferred the oxidation of titanium by cyclic voltammetry, and the resulting equations are as follows:

$$Ti + H_2O \rightarrow TiO + 2H^+ + 2e^- \quad (2)$$

$$2TiO + H_2O \rightarrow Ti_2O_3 + 2H^+ + 2e^- \quad (3)$$

$$Ti_2O_3 + H_2O \rightarrow 2TiO_2 + 2H^+ + 2e^- \quad (4)$$

Table 4. The result of X-ray fluorescence.

Element	Mass% (0 day)	Mass% (15 days)	Mass% (31 days)
Ti	71.47	65.8	65.0
C	8.06	2.41	3.97
Al	5.47	3.69	3.31
V	3.56	2.97	2.98
O	–	13.3	23.0
P	–	0.0329	0.0348
S	–	0.0440	0.234
Fe	–	0.0336	1.24

In order to determine the corrosion products of the Ti–6Al–4V alloy in SRB, the valence state of sulfur, aluminum, and titanium in corrosion products was determined by XPS. Figure 8a–c shows the XPS analysis of the Ti–6Al–4V specimens. XPS analysis of the exposed Ti–6Al–4V specimens with

corrosion products on the surface showed significant peaks for sulfur (S^{2-} and S^{6+}), aluminum (Al^{3+}), and a small amount of titanium (Ti^{4+}). According to Figure 8, sulfates in SRB solution were reduced to sulfides under SRB metabolism as shown by the following reaction [31,32]:

$$H^+ \overset{\text{Hydrogenase}}{\rightarrow} [H] \quad (5)$$

$$SO_4^{2-} + 8[H] \overset{\text{SRB}}{\rightarrow} 4H_2O + S^{2-} \quad (6)$$

S^{2-} and Ti^{4+} will react to form Ti-containing sulfide depositing on the Ti–6Al–4V surface. Then, the electron transfer between the TiO_2 protective film surface and the corrosion product may be enhanced by the sulfide, which accelerated corrosion of the matrix. In addition, the ionization of H_2S may lead to the acidification of the solution. The matrix corrosion process was enhanced by the sulfide accumulation and the electrolyte acidification. Moreover, it is generally accepted that SRB can obtain electrons from metals by direct or indirect contact with metal surfaces. Therefore, there may be an additional corrosion microbattery circuit including anode (steel surface), cathode (bacteria), electron mediator (i.e., nanowire [33] and riboflavin [34]) and ionic medium (solution). It can be reasonably assumed that the electron acquisition process of SRB plays an important role in the corrosion process. Consequently, the sulfide and electron acquisition process is the main mechanism of local corrosion caused by SRB [11]. Rao et al. [10] studied the MIC of ASTM Grade 2 titanium, which proves that the final corrosion product is TiS_2. The increase in corrosion of the aluminum–magnesium alloy may be due to sulfide ions produced by SRB, which will react with aluminum to form aluminum hydroxide, as shown below [32].

$$H_2O \rightarrow H^+ + OH^- \quad (7)$$

$$Al + 3H^+ \rightarrow Al^{3+} + 3[H] \quad (8)$$

$$Al^{3+} + S^{2-} \rightarrow Al_2S_3 \quad (9)$$

$$Al_2S_3 + 6H_2O \rightarrow 2Al(OH)_3 + 3H_2S \quad (10)$$

According to the results determined by the above researchers and the experimental data of this test, it can be inferred that the pitting corrosion process of the Ti–6Al–4V alloy is shown in Figure 9. The results of XRF and XPS analysis are also consistent with the aforementioned articles, so the final corrosion products of the Ti–6Al–4V alloy in SRB solution are a small amount of TiS_2 and $Al(OH)_3$, which indicates that the chemical reaction of aluminum in Ti–6Al–4V is the main cause of the Ti–6Al–4V alloy corrosion in SRB solution.

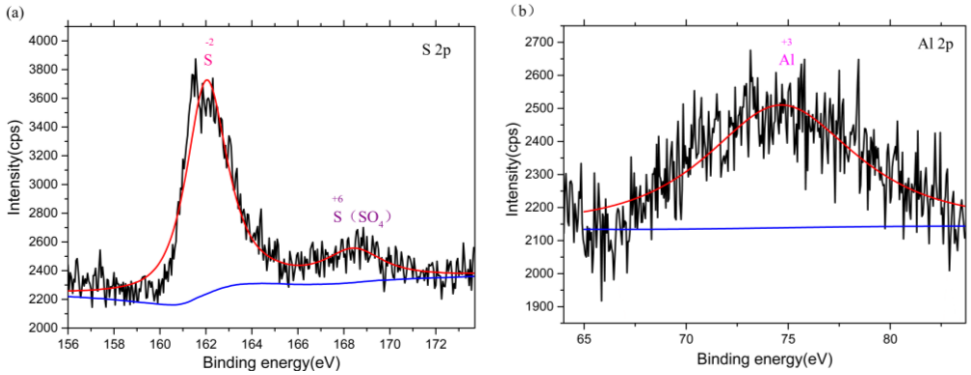

Figure 8. *Cont.*

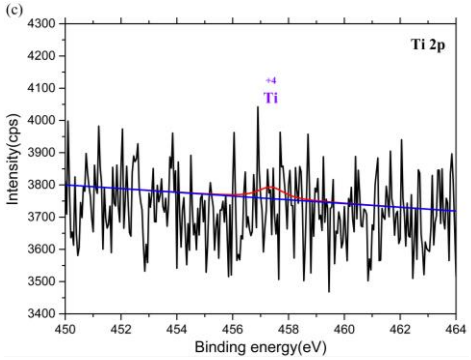

Figure 8. Multiple graphs of the X-ray photoelectron spectroscopy spectra of the three dominant elements coupon exposed to SRB culture. (**a**) sulfur, (**b**) aluminum, and (**c**) titanium.

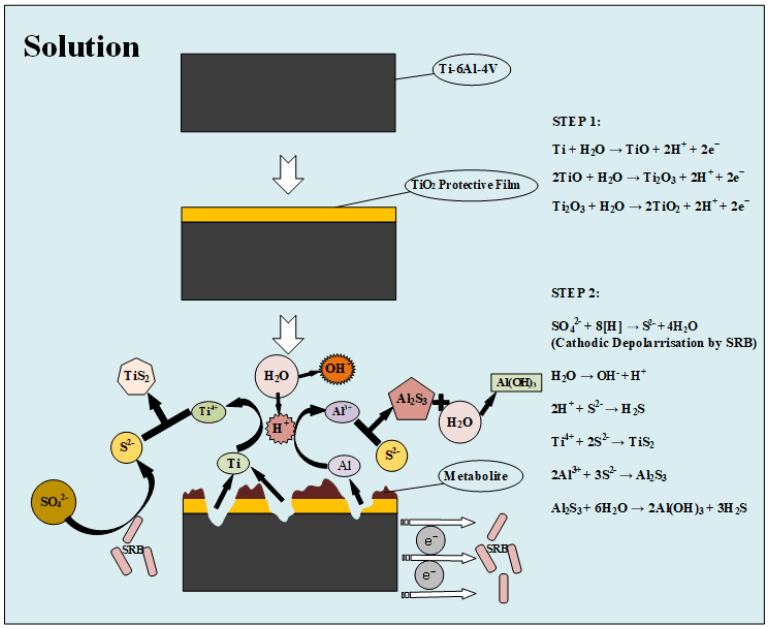

Figure 9. Schematic illustration of a probable mechanism of Ti–6Al–4V alloy corrosion by SRB.

4. Conclusions

This study provides clear evidence for pitting corrosion of the Ti–6Al–4V alloy on exposure to a culture of SRB and theoretical analysis for the application of the Ti–6Al–4V alloy in marine engineering. The following are the key observations and inferences of this study:

- The bacterial adhesion test concludes that SRB will adhere to the surface of the Ti–6Al–4V alloy at a small amount in the initial stage, then colonies will gradually form, and finally, a large amount will adhere to the surface of the Ti–6Al–4V alloy.
- The content of sulfur in the solution increased as the immersion time increased, and a small amount of sulfur has a protective effect on the oxide film on the surface of Ti–6Al–4V. However, as the sulfur element continues to increase, sulfur accelerates the destruction of the oxide film as the immersion time increases.
- SRB metabolites can cause corrosion on Ti–6Al–4V surfaces. The final corrosion product is a small amount of TiS_2 and $Al(OH)_3$, and the chemical reaction of aluminum in Ti–6Al–4V is the main cause of Ti–6Al–4V alloy corrosion.

Author Contributions: Conceptualization, X.Z. (Xingwei Zheng); methodology, Y.L.; software, X.Z. (Xin Zhuang); validation, X.Z. (Xin Zhuang) and Z.C.; formal analysis, J.X. and L.G.; investigation, X.S.; resources, X.Z. (Xingwei Zheng) and Z.C.; data curation, X.Z. (Xin Zhuang); writing—original draft preparation, X.Z. (Xin Zhuang); writing—review and editing, X.Z. (Xingwei Zheng) and Z.C.; visualization, Y.L. and J.X.; supervision, X.Z. (Xingwei Zheng); project administration, X.S.; funding acquisition, X.Z. (Xingwei Zheng) and Z.C. All authors have read and agreed to the published version of the manuscript.

Funding: This work was supported by the National Natural Science Foundation of China (Grant Nos. 51775329 and 51605280) and the Nature Science Foundation of Tianjin City (Grant No. 16JCQNJC03600). Research and verification of rapid detection method for surface trace residues (COMAC-SFGS-2019-301). The development of science and technology of Shanghai Ocean University (No. A2-0203-00-100231), Shanghai Pujiang Program (No. 18PJ1404200), Young Eastern Scholar Program at Shanghai Institutions of Higher Learning.

Acknowledgments: The first author wishes to record his gratitude to Dazhang Yang, College of Food Sciences and Technology, Shanghai Ocean University, for his encouragement and keen interest during the course of this study. The authors are also grateful to Zhitao Shu and Jie Yuan, postgraduates of Shanghai Ocean University, for their constant support during the course of this study.

Conflicts of Interest: The authors declare no conflict of interest.

References

1. Koch, G.H.; Brongers, M.P.H.; Thompson, N.G.; Virmani, Y.P.; Payer, J.H. Chapter 1—Cost of corrosion in the United States. In *Handbook of Environmental Degradation of Materials*; Kutz, M., Ed.; William Andrew Publishing: Norwich, NY, USA, 2005; pp. 3–24.
2. Fragata, F.; Salai, R.P.; Amorim, C.; Almeida, E. Compatibility and incompatibility in anticorrosive painting: The particular case of maintenance painting. *Prog. Org. Coat.* **2006**, *56*, 257–268. [CrossRef]
3. Li, Y.C.; Xu, D.K.; Chen, C.F.; Li, X.G.; Jia, R.; Zhang, D.W.; Sand, W.; Wang, F.H.; Gu, T.Y. Anaerobic microbiologically influenced corrosion mechanisms interpreted using bioenergetics and bioelectrochemistry: A review. *J. Mater. Sci. Technol.* **2018**, *34*, 1713–1718. [CrossRef]
4. Rao, T.S.; Sairam, T.N.; Viswanathan, B.; Nair, K.V.K. Carbon steel corrosion by iron oxidising and sulfate reducing bacteria in a freshwater cooling system. *Corros. Sci.* **2000**, *42*, 1417–1431. [CrossRef]
5. Rao, T.S.; Nair, K.V.K. Microbiologically influenced stress corrosion cracking failure of admiralty brass condenser tubes in a nuclear power plant cooled by freshwater. *Corros. Sci.* **1998**, *40*, 1821–1836. [CrossRef]
6. Tatnall, R.E.; Stanton, K.M.; Ebersole, R.C. Test for the presence of sulfate reducing bacteria. *Gen. Interest* **1988**, *27*, 71–80.
7. Iverson, W.P. Research on the mechanisms of anaerobic corrosion. *Int. Biodeter. Biodegr.* **2001**, *47*, 63–70. [CrossRef]
8. Venzlaff, H.; Enning, D.; Srinivasan, J.; Mayrhofer, K.J.J.; Hassel, A.W.; Widdel, F.; Stratmann, M. Accelerated cathodic reaction in microbial corrosion of iron due to direct electron uptake by sulfate-reducing bacteria. *Corros. Sci.* **2013**, *66*, 88–96. [CrossRef]
9. Liu, F.L.; Zhang, J.; Zhang, S.T.; Li, W.H.; Duan, J.Z.; Hou, B.R. Effect of sulfate reducing bacteria on corrosion of Al–Zn–In–Sn sacrificial anodes in marine sediment. *Mater. Corros.* **2012**, *63*, 431–437. [CrossRef]
10. Rao, T.S.; Kora, A.J.; Anupkumar, B.; Narasimhan, S.V.; Feser, R. Pitting corrosion of titanium by a freshwater strain of sulfate reducing bacteria (*Desulfovibrio vulgaris*). *Corros. Sci.* **2005**, *47*, 1071–1084. [CrossRef]
11. Wu, T.Q.; Yan, M.C.; Yu, L.B.; Zhao, H.T.; Sun, C.; Yin, F.C.; Ke, W. Stress corrosion of pipeline steel under disbonded coating in a SRB-containing environment. *Corros. Sci.* **2019**, *157*, 518–530. [CrossRef]
12. Jia, R.; Wang, D.; Jin, P.; Unsal, T.; Yang, D.Q.; Yang, J.K.; Xu, D.K.; Gu, T.Y. Effects of ferrous ion concentration on microbiologically influenced corrosion of carbon steel by sulfate reducing bacterium Desulfovibrio vulgaris. *Corros. Sci.* **2019**, *153*, 127–137. [CrossRef]
13. Erinosho, M.F.; Akinlabi, E.T.; Pityana, S. Microstructure and corrosion behaviour of laser metal deposited Ti–6Al–4V/Cu composites in 3.5% sea water. *Mater. Today Proc.* **2015**, *2*, 1166–1174. [CrossRef]
14. Gorynin, I.V. Titanium alloys for marine application. *Mater. Sci. Eng. A* **1999**, *263*, 112–116. [CrossRef]
15. Toque, C.; Milodowski, A.E.; Baker, A.C. The corrosion of depleted uranium in terrestrial and marine environments. *J. Environ. Radioact.* **2014**, *128*, 97–105. [CrossRef]
16. Pillay, C.; Lin, J. The impact of additional nitrates in mild steel corrosion in a seawater/sediment system. *Corros. Sci.* **2014**, *80*, 416–426. [CrossRef]

17. Batt, C.; Dodson, J.; Robinson, M. Hydrogen embrittlement of cathodically protected high strength steel in sea water and seabed sediment. *Br. Corros. J.* **2002**, *37*, 194–198. [CrossRef]
18. Yang, X.J.; Du, C.W.; Wan, H.X.; Liu, Z.Y.; Li, X.G. Influence of sulfides on the passivation behavior of titanium alloy TA2 in simulated seawater environments. *Appl. Surf. Sci.* **2018**, *458*, 198–209. [CrossRef]
19. Coyer, J.A.; Cabello-Pasini, A.; Swifi, H.; Alberte, R.S. N_2 fixation in marine heterotrophic bacteria: Dynamics of environmental and molecular regulation. *Proc. Natl. Acad. Sci. USA* **1996**, *93*, 3575–3580. [CrossRef]
20. Oguro, A.; Kakeshita, H.; Takamatsu, H.; Nakamura, K.; Yamane, K. The effect of Srb, a homologue of the mammalian SRP receptor α-subunit, on Bacillus subtilis growth and protein translocation. *Gene* **1996**, *172*, 7–24. [CrossRef]
21. Li, D.G.; Wang, J.D.; Chen, D.R.; Liang, P. Influence of passive potential on the electronic property of the passive film formed on Ti in 0.1 M HCl solution during ultrasonic cavitation. *Ultrason. Sonochem.* **2016**, *29*, 48–54. [CrossRef]
22. Nowak, W.B.; Sun, E.X. Electrochemical characteristics of Ti–6Al–4V alloy in 0.2 N NaCl solution: II. Kinetic behaviors and electric field in passive film. *Corros. Sci.* **2001**, *43*, 1817–1838. [CrossRef]
23. Sikora, E.; Macdonald, D.D. Nature of the passive film on nickel. *Electrochim. Acta* **2002**, *48*, 69–77. [CrossRef]
24. Bai, Y.; Gai, X.; Li, S. Improved corrosion behaviour of electron beam melted Ti–6Al–4V alloy in phosphate buffered saline. *Corros. Sci.* **2017**, *123*, 289–296. [CrossRef]
25. Danilov, V.A.; Tade, M.O. An alternative way of estimating anodic and cathodic transfer coefficients from PEMFC polarization curves. *Chem. Eng. J.* **2010**, *156*, 496–499. [CrossRef]
26. Zhang, X.P.; Chen, G. Corrosion protecttion of AZ91D Mg alloy coating with micro-arc oxidation film evaluated by immersion and electrochemical tests. *Sur. Rev. Lett.* **2005**, *12*, 279–287. [CrossRef]
27. Shi, M.L. *Principle and Application of AC Impedance Spectroscopy*; National Defense Industry Press: Beijing, China, 2000.
28. Cheng, X.L.; Ma, H.Y.; Chen, S.H.; Chen, X.; Yao, Z.M. Corrosion of nickel in acid solutions with hydrogen sulphide. *Corros. Sci.* **2000**, *42*, 299–311. [CrossRef]
29. Pourbaix, M. A comparative review of electrochemical methods of assessing corrosion and the behaviour in practice of corrodible material. *Corros. Sci.* **1965**, *5*, 677–700. [CrossRef]
30. Cocke, D.L.; Hess, T.R.; Mebrahtu, T.; Mencer, D.E.; Naugle, D.G. The surface reactivity of $Ti_{36}Cu_{64}$ and $Ti_{36}Al_{64}$ alloys and the ion chemistry of their oxide overlayers. *Solid State Ion.* **1990**, *43*, 119–131. [CrossRef]
31. Jia, R.; Tan, J.L.; Jin, P.; Blackwood, D.J.; Xu, D.K.; Gu, T.Y. Effects of biogenic H_2S on the microbiologically influenced corrosion of C1018 carbon steel by sulfate reducing Desulfovibrio vulgaris biofilm. *Corros. Sci.* **2018**, *130*, 1–11. [CrossRef]
32. Liu, J.H.; Liang, X.; Li, S.M. Study of microbiologically induced corrosion action on Al–6Mg–Zr and Al–6Mg–Zr–Sc. *J. Rare Earths* **2007**, *25*, 609–614.
33. Sherar, B.W.A.; Power, I.M.; Keech, P.G.; Mitlin, S.; Southam, G.; Shoesmith, D.W. Characterizing the effect of carbon steel exposure in sulfide containing solutions to microbially induced corrosion. *Corros. Sci.* **2011**, *53*, 955–960. [CrossRef]
34. Zhang, P.; Xu, D.; Li, Y.; Yang, K.; Gu, T. Electron mediators accelerate the microbiologically influenced corrosion of 304 stainless steel by the Desulfovibrio vulgaris biofilm. *Bioelectrochemistry* **2015**, *101*, 14–21. [CrossRef] [PubMed]